Drying Technology
An International Journal

ISSN: 0737-3937 (Print) 1532-2300 (Online) Journal homepage: http://www.tandfonline.com/loi/ldrt20

Use of Hyperspectral Imaging for the Prediction of Moisture Content and Chromaticity of Raw and Pre-Treated Apple Slices during Convection Drying

Stuart Crichton, Luna Shrestha, Anya Hurlbert & Barbara Sturm

To cite this article: Stuart Crichton, Luna Shrestha, Anya Hurlbert & Barbara Sturm (2017): Use of Hyperspectral Imaging for the Prediction of Moisture Content and Chromaticity of Raw and Pre-Treated Apple Slices during Convection Drying, Drying Technology, DOI: 10.1080/07373937.2017.1356847

To link to this article: http://dx.doi.org/10.1080/07373937.2017.1356847

Accepted author version posted online: 27 Jul 2017.

Use of hyperspectral imaging for the prediction of moisture content and chromaticity of raw and pre-treated apple slices during convection drying

Stuart Crichton

Postharvest Technologies and Processing Group, Department of Agricultural Engineering, University of Kassel, Witzenhausen, Germany

Luna Shrestha

Postharvest Technologies and Processing Group, Department of Agricultural Engineering, University of Kassel, Witzenhausen, Germany

Anya Hurlbert

Institute of Neuroscience, Newcastle University, Newcastle upon Tyne, UK

Barbara Sturm

Postharvest Technologies and Processing Group, Department of Agricultural Engineering, University of Kassel, Witzenhausen, Germany

School of Agriculture, Food and Rural Development, Newcastle University, Newcastle upon Tyne, UK

Address correspondence to Barbara Sturm. E-mail: barbarasturm@daad-alumni.de

ABSTRACT

The feasibility of using spectral reflectance information in the visible – near infra-red (400-1000 nm) region to estimate moisture content (g_W/g_{DM}) and chromaticity (*CIELAB*) of apple slices was investigated during convection drying. Apple slices were pre-treated with hot water blanching (50°C and 70°C), acid application (citric and ascorbic) and combinations thereof before drying at 50°C and 70°C. Prediction models for the space-averaged spectral reflectance curves were built using the partial least square regression method. A three-component PLSR model satisfied the minimal RMSE criterion for predicting moisture content (Avg. RMSEP = 0.13, r^2 = 0.99); importantly, the critical wavelengths remained the same across all pre-treatments [540 nm, 817 nm, 977 nm]. Similarly, PLSR modelling showed that the optimal set of wavelengths (in terms of RMSE) were invariant across pre-treatment for *CIELAB a** prediction [543 nm, 966 nm], and *CIELAB b** prediction [510 nm, 664 nm, 714 nm, 914 nm, 969 nm]. The stability of the information content of these wavelengths across pre-treatments indicates their independence of colour changes. Additionally, the spatial information in the hyperspectral images was exploited to visualise the performance of the predictive models by pseudo-colouring their values for each pixel in a single apple slice across different drying times. This visualisation of the spatial distribution of predicted moisture content and chromaticity changes shows significant potential for use in online monitoring of the drying process.

KEYWORDS: apples, chromaticity, hyperspectral, moisture content, pre-treatments

1. Introduction

Despite its wide-spread use and importance, the drying process in general is still imperfectly understood, in terms of the influence of and interaction between different conditions,[1]

and non-optimally controlled.[2,3] In conventional drying applications, for example, process settings, technologies and control systems are based on parameter scheduling, without real-time feedback from the monitoring of product characteristics, such as surface temperature or moisture content, which have been shown to influence both product quality and drying behaviour.[4–8] This lack of adaptive control has far-reaching implications for the product quality achieved as well as for process- and resource-efficiency and sustainability aspects. To ensure output product quality under these restrictive conditions, the quality of raw materials entering the processing stage is usually tightly controlled, resulting in unnecessarily high losses upstream, with a high proportion of produce rejected for being outside pre-determined boundaries. In addition to this output inefficiency, drying is also energy-inefficient, with efficiencies on average approximately 35-45% but in some cases falling as low as 10%.[9] Given that drying is responsible for 15-25% of the overall industrial energy demand across all sectors,[6] there is a strong need to improve the energy-efficiency of drying while also reducing food wastage.

The production of dried apple products, such as slices and powders, relies on removal of water to below a specific threshold water content. Nonetheless, achieving the target moisture content does not, on its own, ensure that the dried produce will be appealing to the consumer. The main focus of consumers is on the visual appearance, or other sensory properties, of the product, which consumers relate to overall product quality, and which directly influence their purchasing behaviour.[10–12] Rejection of food products on the basis of aesthetic or safety concerns is often cited as the major cause of food losses and waste, particularly in fruit and vegetable (F&V) commodities (≤45%).[13] Therefore, in optimising the drying process for energy efficiency and product conservation, it is also desirable to preserve the visual appearance of a product as much as possible.

A major goal for the drying industry is therefore to develop a system in which the drying process is adaptively optimised for energy efficiency, product conservation and product quality, simultaneously, via online and inline non-destructive monitoring of product quality metrics, and the integration of feedback from such monitoring into process control[14]. Su et al.[14] comprehensively review methods suitable for such "smart drying" systems. The central component for such a system is the real-time estimation of moisture content. Much effort has been focused on methods to estimate moisture content of different food products, both inside and outside of processing stages. The gravimetric method allows for the moisture content of a tray of produce to be estimated non-invasively during the drying process, but the estimate applies only to the entire tray, rather than to individual product particles, whose moisture content might therefore vary above or below the target value. Furthermore, to validate the moisture content estimates, which are based on weight changes during drying, a representative sample must be used for final dry matter determination at the end of the process (following the American Association of Official Analytical Chemists),[15] or, alternatively, individual samples must be removed and their current moisture content determined using destructive methods (i.e. the quick test). The gravimetric method is not viable in most industrial dryers since the integration of balances is not possible, and thus, the current moisture content needs to be evaluated using the destructive quick test. The individual products used for these determinations might need then to be discarded or further processed for other purposes, leaving the wastage problem unsolved.

Non-contact, non-destructive methods for moisture content estimation include biomimetic systems, computer vision technology, microwave dielectric spectroscopy, near infrared reflectance (NIR) spectroscopy, magnetic resonance imaging (MRI), ultrasonic techniques, electrostatic sensor technology and control systems for drying environments[14,16,17] via devices which, in

combination with moveable areas of focus, enable moisture content sampling of individual products over a period of time. Like the technique of NIR spectroscopy,[18] widely-used for moisture content estimation due to the high absorption of NIR wavelengths by water,[19] these methods provide low spatial resolution.

Optical methods, on the other hand, are also non-destructive and non-contact, and offer the opportunity of high spatial resolution in conjunction with the ability to analyse each sample individually and to visualise moisture content variation across individual samples. Optical methods such as laser light backscattering methods[20,21] have also been used. In the last 10 years, though, hyperspectral imaging (HSI) has been intensively used in the food processing industry,[22,23] offering the high spectral resolution of spectroscopy, combined with the high spatial resolution of optical imaging devices. In comparison to the overall hyperspectral imaging literature, though, the use of hyperspectral imaging with regards specifically to drying is relatively underexplored,[25–34] with only a subset of HSI drying studies specifically tackling moisture content estimation.[35] While the use of hyperspectral imaging in the NIR range for estimating water content is clearly desirable and powerful, and has been successfully used for some processes such as the drying of salted meat,[29] it is also expensive, in comparison to VNIR (400-1000nm) imaging, due to the cost of sensors. Investigations into the feasibility of moisture content estimation using HSI in the VNIR region are therefore of great interest. Previous studies using HSI-VNIR measurements during drying have related acquired spectral signals to colour and moisture content, using produce which does not require pre-treatment (e.g. soybeans[25] and meat[36,37]), or using drying methods which minimise colour change.[31] Commercial drying processes for many products do, though, use different pre-treatments to minimise colour and shrinkage changes.[3,38] It is important, therefore,

to examine the effects of common treatments such as blanching on VNIR spectral signals, given the obvious (intended) effects of blanching in the visible wavelength region.

Apples are of particular importance in this context. They are common commodities in the dried fruit market, typically subjected to different pre-treatments to reduce discolouration during drying, and typically produced using traditional convection driers without automated process control. Depending on the target market, consumers' expectations of dried apple quality differ greatly. Standard mass produced products are expected to be practically unchanged with regard to colour in comparison to the fresh produce. The organic market however, accepts or even almost expects a certain degree of changes in colour, provided no artificial additives have been used to reduce colour changes which might occur during preparation and/or drying.

The focus of this investigation is therefore on the changes in surface spectral reflectance of apples during the drying process, obtained via hyperspectral imaging, with the specific aims: (1) to determine how these are affected by different pre-treatments (prior to drying) which are designed to affect the visual appearance of the final product; (2) to extract from the hyperspectral reflectance measurements key parameters which relate to moisture content and (3) to consider the feasibility of using such parameters to provide online control of the drying process for a variety of input materials.

2. Material and Methods

Apples of the variety Golden Delicious were sourced from a local supermarket after visual assessment of uniformity in ripeness and size. The apples were then stored at room temperature until the experiments were conducted. To prepare slices, the initial 1.5 cm of each apple, from the stalk region, was discarded and the following three successive 5 mm slices were utilised for

experiments. The peel was kept on the apple slices. Pre-treatments included blanching at 50°C and 70°C for 4 min, use of ascorbic and citric acid (1%) and combinations thereof; these were applied before drying apple slices at 50°C and 70°C. These pre-treatments were selected to fill gaps identified in previous studies.[39,40] Apple pre-treatments and process settings are summarised in **Table 1** below, where HWB denotes hot water blanching, ASC denotes ascorbic acid blanching (1%), and CIT denotes citric acid blanching (1%).

This procedure results in samples of three slices per treatment condition, with a total sample number of 30 slices. Apple slices were placed directly onto a uniformly black translation stage. The physical size of the slices averaged 70 mm in diameter, with an average area of 3847 mm^2 after removal of the core. Each complete image consisted of 3 apple slices and the white reference tile. Given the imaging parameters of the camera setup (**Figure 2**), the average number of pixels captured for each individual apple slice was around 130,000, prior to ignoring the core region, meaning that each pixel has a spatial area of 0.03 mm^2.

2.1. Weight and colorimetric measurements

Drying was undertaken using a convective air cabinet dryer at the University of Kassel, Witzenhausen, Germany (HT-Mini, Innotech Ingenieurgesellschaft mbH, Altdorf, Germany), which allowed for control of air temperature (±2°C), with a fixed air speed. Weight measurements were conducted using a Sartorius Excellence E2000D (Sartorius AG, Göttingen, Germany). Colorimetric values were recorded using a Konica Minolta CR-400 (Konica Minolta, Japan).

2.2. Hyperspectral image capture

All hyperspectral images were acquired using a Specim V10E PFD camera (Specim Spectral Imaging Ltd., Finland, via LOT-QuantumDesign GmbH, Germany) fitted with a

Schneider 35 mm lens (Xenoplan 1.9/35, Schneider Optische Werke GmbH, Germany) and coupled to a linear translation stage (Specim Spectral Imaging Ltd., Finland). Illumination was provided by 3 60W halogen GU10 bulbs with the illumination spectrum shown in **Figure 1**. Halogen bulbs offer the advantage of having a very stable spectral and power output, requiring no warm up period.

This set up allowed the capture of spectral data from 400-1010 nm, in 1.5 nm increments. The white reference tile measured 200 mm* 24 mm (W*H), with an overall image spatial resolution of 1632 by 1302 pixels (H*W). The translation stage moved at a speed of 8 mm/s. Samples were imaged as shown in **Figure 2** below.

2.2.1. Image processing

After capture, automatic processing of the irradiance images was undertaken. The first stage was removal of the estimated dark noise from the raw image irradiance, carried out by calculating the spatial mean signal at each wavelength in the dark noise file and subtracting these values from the respective hyperspectral sample image files:

$$MDN_{\lambda} = \left(\frac{\sum_{N} I_{DN_{\lambda}}}{N} \right) \qquad (1)$$

$$\bar{I}(\lambda_{x,y}) = I(\lambda_{x,y}) - MDN_{\lambda} \qquad (2)$$

Here, MDN_{λ} is the mean value at the specified wavelength λ of the calculated dark noise (DN); $I_{DN_{\lambda}}$ is the raw DN value at that wavelength at a given pixel; N is the total number of pixels in the DN file; $I(\lambda_{x,y})$ is the raw image irradiance; and $\bar{I}(\lambda_{x,y})$is the dark-noise-corrected image irradiance.

The second stage was the automatic detection and segmentation of the apple slices and white reference tile from the background, using the dark-noise-corrected image. All image processing was undertaken using an in-house toolbox at Agrartechnik, Universität Kassel, based upon one from the Institute of Neuroscience, Newcastle University, written and implemented within the Matlab software package (Matlab R2013a). This software first segments the samples and white reference from the image background by averaging the NIR irradiance spectrum (800-1010 nm) for each pixel, and applying a threshold function to these average NIR pixel values. The NIR region, rather than the visible spectrum, was used for segmentation because of the lower irradiance of the background in this region. An example of the segmentation for a complete image is shown below, with the original RGB image, the NIR segmented region, and the final segmented image with pseudo-coloured blobs corresponding to apple slices and white reference.

The aim of the following stage was to obtain the reflectance image of the apple slices, for which the illumination spectrum at each location in the slice image must first be calculated. Due to the use of a linear scanner and the non-uniformity of the illumination across the imaging field, the illumination spectrum varied in the horizontal dimension of the final image (as depicted in **Figure 3**). The average illumination ($W(\lambda_x)$) was therefore calculated for each column in the image as the average dark-noise-corrected irradiance of the corresponding column in the white reference tile at the bottom of the image. The relative reflectance spectrum for each pixel in the image ($R(\lambda_{x,y})$) was then calculated by removing the column-dependent illumination spectrum ($W(\lambda_x)$) from the irradiance spectrum ($\bar{I}(\lambda_{x,y})$) by simple division;

$$R(\lambda_{x,y}) = \frac{\bar{I}(\lambda_{x,y})}{W(\lambda_x)} \qquad (3)$$

Using a logical AND operator with the segmented images (as shown in **Figure 3**b and c) to restrict the image data to regions with material slice content only, the average reflectance spectra R(λ) for each apple slice sample was calculated from the relative reflectance image ($R(\lambda_{x,y})$). The calculated average reflectance spectra were then analysed using PLSR in relation to a number of quality metrics: moisture content (g/ g), *CIELAB a** and *CIELAB b**. Due to the lower emission of the halogen bulbs between 400-500 nm all PLSR analysis was undertaken within the spectral range of 500 nm – 1010 nm.

2.2.2. Use of spectral pre-processing

The raw reflectance signal, obtained by factoring out the spatially-varying illumination signal as described above, may under some conditions require further processing to remove distortions caused by, for example, the effects of shadows, different particle sizes or scattering of the incident illumination within the surface of the sample. At times these methods are applied in an attempt to improve model classification by decontaminating the images (see[41] for an analysis of the effect of different spectral pre-processing methods on the resulting model accuracy), but, as Amigo et al.[42] state, much care and thought needs to be taken prior to use, given the potential of certain scatter-correcting or derivative operations to introduce shape changes to the spectra. Previous studies[42,43] have also investigated the use of different spectral pre-processing algorithms on the raw irradiance spectra for each pixel, prior to calculation of reflectance and averaging. In general, the need to use different pre-processing techniques is related to both the physical nature of the sample being imaged, and the electromagnetic wavelength region being measured. For example, samples with a varied texture, which results in scattering and shadowing on the surface, require pre-processing techniques to minimise the effects of these phenomena on the raw image irradiance or recovered surface reflectance. In this study, though, the apple slices tested have a

relatively smooth surface. In addition, the combination of perpendicular illumination source, the use of the VNIR region, and the opacity of the sample, also minimises any problems caused by sub-surface scattering of the test illumination within the apple slices. Therefore, pre-processing methods to counteract scattering effects are not required. Other pre-processing techniques include derivative-based techniques, which may be used to highlight or extract important spectral features in the retrieved spectra.[42] These techniques may be useful if any spectral features being investigated are very narrowband and relatively small in amplitude. In this study, again, the need for derivative techniques to extract signals of interest is minimal, given that reflectance spectra in the VNIR are generally very smooth and more broadband in nature than those in the NIR or IR regions.

The decision to use the relative reflectance format for representing the spectra in this study has also been taken after consideration of alternative formats. Generally, most investigations utilise the relative reflectance representation,[31,44–49] although other representations, such as absorbance, do exist,[50] and may be used for spectra which have not under gone derivative processing. In fact, the reflectance and absorbance formats may be considered as uniform translations of each other. The use of Kubelka-Munk (K-M) units,[51] into which reflectance spectra may be converted,[50] is a different approach. K-M theory was proposed to explain the spectral characteristics of colourants such as dyes on paper. Its applicability is constrained, though, by a number of environmental assumptions, ranging from the assumption of completely diffuse illumination, to the surface under measurement being a flat plane and the colourants being a separate layer. Its main spectral region of applicability is the visible region (400-780 nm). When applied to foodstuffs, a number of the assumptions can be seen to be problematic, especially in conjunction with surface profile changes

during processing.[33,49,52] Furthermore, a comparative analysis of approaches based on these three different formats,[48] showed that no real performance difference existed.

With these considerations in mind, the approach taken in this work uses the raw relative reflectance data only, acquired following the steps in section 2.2.1, as the basis for the PLSR models. The results demonstrate that this approach results in a high level of model accuracy.

3. Experimental Methodology

For each apple treatment, apple slices were imaged, weighed and colorimetrically measured every 30 minutes during the drying process, up to 180 minutes, and subsequently each 60 minutes up to a total of 300 minutes. At each measurement time point, samples were briefly removed from the test oven for the measurement process, resulting in 9 measurements per slice (0, 30, 60, 90, 120, 150, 180, 240 and 300 minutes) and 27 measurements in total for each treatment condition except the two control groups (conditions 1 and 2; 0 – 240 minutes), for which there were 24 measurements each. The control groups were dried up to 240 minutes only, in order to investigate a minimum drying time for the experimental apple slices.

3.1 Moisture content measurement

Moisture content was calculated using the thermo-gravimetric method. For the determination of dry matter content (M_0), the samples were placed into an electrical oven (Memmert Model 500, Memmert GmbH + Co.KG, Schwabach, Germany) at a constant temperature of 70°C for an additional 48h following the final measurement, then weighed. Dry basis moisture content of the samples at each time point (MC_t) throughout the drying experiments was calculated from the measured mass at each time point (M_t) using following equation;

$$MC_t = 100 * \frac{(M_t - M_0)}{M_t} \qquad (4)$$

3.2 Modelling technique

The aim of modelling is to extract from the dense hyperspectral reflectance image data a smaller set of reflectance values, at a small number of critical wavelengths, which reliably predict moisture content at each time point. For this purpose, we used standard Partial Least Squares (PLS) regression [53] to construct predictors for moisture content from the averaged relative reflectance spectra by maximising the variance explained, (r^2), in projected spaces for both, for each treatment condition separately. The optimal number of components of the PLSR model is typically determined by minimising RMSE and maximising r^2.[54] Here, after examining the effects of varying numbers of components on PLSR model performance, we selected the most critical wavelengths related to prediction of moisture content and chromaticity to further reduce the number of model components, guided by RMSE and r^2. RMSE is calculated as the root-mean-squared average difference between predicted (MC_{pred}) and measured (MC_{meas}) moisture content at each time point. These reduced models were then tested with the dataset.

4. Results

4.1. Moisture content prediction

Previous applications of combining time-series hyperspectral imaging with drying have investigated produce under only a single drying condition.[25,31,33] Although investigations into moisture content prediction of other foodstuffs, such as bananas, have introduced variations in produce through the use of maturation,[55] the effects of variations due to common product pre-treatments on the estimation models have not been investigated. A key aim of this study is therefore

to examine the effects of the distinct pre-treatment conditions on the regression models for moisture content prediction.

The variation in reflectance spectra with different pre-treatments is evident in the initial measurements (**Figure 4a**) as well as other time points (**Figure 4b**), although the shape of the spectra remains broadly similar across all treatments, with the prominent dip around wavelength ~680 nm, likely corresponding to *chlorophyll a* absorbance,[25,56] persisting at the 180 minutes time point. The variation in reflectance spectra with time during the drying process for a given treatment condition (**Figure 5a**; condition 1) shows clearly that in addition to changes in relative reflectance within the visible spectrum, reflectance peaks in the NIR region are significantly affected by drying.

The initial PLSR analyses were carried out on the full reflectance spectra. The complete dataset of 53 measured spectra (24 measurements for the control groups; 29 measurements for the remaining conditions) was then split on a 2:1 ratio for the calibration and test sets, with 2 apples randomly assigned to the calibration set, and 1 to the test set. The two data sets were therefore built using measurements from different slices. For each treatment condition, PLSR was performed for models with component numbers varying from 1-20, and for each of these, model creation and testing were performed 10 times. The ten distinct loading functions, one for each treatment condition, for the 4-component PLSR model (obtained by averaging the loading functions for each of the 10 model runs) are shown in **Figure 5b**. Despite the initial differences in reflectance spectra across conditions, it is clear that the loading functions emphasise the same set of wavelengths, with only the weights on these wavelengths varying across conditions in the calculated models with the same number of components.

The three-component PLSR model satisfied the minimal RMSE criterion, leading to the selection of a reduced set of critical wavelengths, [540nm, 817nm, 977nm]; these also correspond to the wavelengths with largest loadings as seen in the 4-component model (**Figure 5b**). The average results of the models obtained from the initial PLSR on the full spectra, for each treatment, together with the average performance of the 3-component reduced-set treatment models are shown in **Table 2**.

4.2. CIELAB chromaticity prediction

The same methodology was utilised to investigate the feasibility of *CIELAB a** and *b** prediction from descriptors extracted from the hyperspectral reflectance data. Again, the critical wavelengths identified as important remained the same across the 10 treatment conditions. PLSR modelling showed that 2 wavelengths provided the best performance (in terms of RMSE) for *CIELAB a** prediction [543nm, 966nm], and 5 for *CIELAB b** prediction [510nm, 664nm, 714nm, 914nm, 969nm]. The model results for both colour appearance components are shown below.

5. Discussion

The results of the predictive modelling of the three metrics demonstrate good performance with large reductions in the number of wavelengths required, from the full VNIR spectrum of 500-1010nm down to minimal sets of 2-5 wavelengths. Predictive modelling of moisture content showed the importance of 3 wavelengths [540 nm, 817 nm, 977 nm], irrespective of the existence or type of pre-treatment. The stability of the information content of these wavelengths across pre-treatments indicates their independence of colour changes. This fact is one which needs to be considered when developing models which utilise imaging in the visible wavelength range. The

spectral locations of these wavelengths show that both the "green" region of the visible range and the NIR region are important and can be utilised to estimate moisture content.

The performance of the low-component PLSR models developed here is difficult to compare directly with previous attempts to monitor moisture content during apple drying, largely because of the lack of such studies or their use of different error metrics. The most directly comparable study, which uses a laser backscattering system to estimate moisture content,[21] reports a standard error of cross-validation (SECV) of 9.8% and a correlation coefficient of r^2 = 0.89 for the model using light luminescence to predict moisture content. The worst performance of the latter model is for moisture contents of between 10-20%, where prediction errors are clearly on the order of the moisture content value itself; lower moisture contents are not validated with this technique.[21] By comparison, the worst performance of the PLSR models developed here on the basis of HSI data, occurring for Condition 7, is characterised by a correlation coefficient of r^2 = 0.98, with a mean model error for the predicted moisture content of 0.29 g_W/g_{DM}, or 3.49% (see **Table 2**). The moisture content development of the investigated samples is shown in **Table 5**. Comparing this moisture content value with the change in measured moisture content over drying time for Condition 7 (**Figure 6a**), it is clear that the three-component PLSR model therefore performs accurately (in terms of RMSE) for drying times up to 90 minutes, and moisture contents down to around $0.1 g_W/g_{DM}$. Because this value is the target value for moisture content, the flattening of the drying curve (which accounts for the increase in RMSE) does not adversely affect the target period of drying.

The developed models for *CIELAB* a^* and b^* also both show a good level of performance across all treatment conditions. Both of the PLSR models for chromaticity co-ordinate prediction

utilise NIR wavelengths within their models, demonstrating that it is not only wavelengths within the expected visible region that directly predict the chromatic properties.

The colour of an apple is caused by a combination of different pigments within the flesh.[56] During drying, as moisture leaves the flesh of an apple, and if we assume minimal pigment loss, the concentration of these pigments will increase, leading to changes in colour. Changes in apple colour might also be due to enzymatic reactions as a consequence of oxidation of different phenolic compounds present in apples and/or due to Millard reactions during the drying process.[58,59] For example, Yemeniciglu et al.[60] observed that polyphenol oxidase enzymes in the golden delicious apple variety are completely deactivated at 68°C. However, this processing temperature is not reached until the end of the drying process.[61] These changes in apple colour are controlled by using different pre-treatments.[59,62–68].

Given that the original hyperspectral images for each apple slice at each drying time contain the full reflectance spectra at each pixel location, we may also use these data to extract the predicted moisture content and chromaticity coordinates for each pixel using the final reduced-set PLSR models, and visualise the performance of the models for the three metrics by pseudo-colouring their values for each pixel in a single apple slice across different drying times. **Figure 7** shows the resulting pseudo-colour images for the predicted moisture content and chromaticity coordinates in comparison with the sRGB images created from the hyperspectral image, for a single apple slice at two different drying times.

The spatial variation of the 3 quality metrics over the first 60 minutes of drying at 50°C is apparent in the pseudo-colour images (**Figure 7**). The spatial distribution of moisture within the slice can be seen to retreat towards the core during drying. The variation in the spatial distribution of predicted *CIELAB a** values over the drying time allows features such as veins to become more

apparent [**Figure 7**c, g, h]. The variation in the spatial distribution of predicted *CIELAB b** values, on the other hand, is smaller over drying time, with the greatest change occurring in the peel, visible as the bright rim at both drying times. As drying progresses, the slice deforms and the peel becomes more visible. At 60 minutes (**Figure 7h**), the rim develops more extreme values, seen especially along the top edge of the apple slice in **Figure 7h** , due to the more specular nature of the reflected spectrum within this region. Overall, the spatial maps of predicted apple characteristics during drying provide high quality information, and, especially when co-registered with the sRGB image, supplements and gives more detail about particular visible features relevant to decision-making on product quality.

6. Conclusions

This investigation demonstrates that VNIR hyperspectral imaging, and specifically the image data at a reduced number of specific wavelengths, can be used to accurately determine moisture content and *CIELAB* chromaticity co-ordinates of apple slices during drying. PLSR modelling demonstrates that reflectance data at 3 specific wavelengths are sufficient to predict moisture content, with 2 and 5 wavelengths required to estimate *CIELAB a* and b** values respectively. The spectral location of these critical wavelengths remains stable across all apple treatments, including blanching to minimise chromatic changes during drying, and therefore these wavelengths may be considered as treatment-invariant wavelengths for the investigated quality metrics. Because the hyperspectral imaging technique provides full spectral data at each pixel, the derived PLSR models allow visualisation of the predicted moisture content and chromaticity changes across the entire apple slices. Spatial inhomogeneities in the quality metrics over the drying time are readily visualised. The next stage of work will be to incorporate these findings into a simplified optical system for real time monitoring of these metrics during drying.

Acknowledgements

The authors wish to thank the Core Organic Plus Programme for the financial support within the SusOrganic project (project number BLE-2814OE006); the Newcastle Institute for Research on Sustainability for their support via the NIRES Responsive Mode Grant BH149667 and the University of Kassel for their financial support in the framework of the Nachwuchsgruppen programme.

Abbreviations

ASC: Ascorbic acid

CIT: Citric acid

DM: Dry Matter

F&V: Fruit and vegetable

HSI: Hyperspectral imaging

HWB: Hot water blanching

K-M: Kubelka-Munk

MC: Moisture content

MRI: Magnetic Resonance imaging

PLSR: Partial least squares regression

RMSE: Root mean square error

SECV: Standard error of cross validation

VNIR: Visual to near infra-red

W: water

< bodyend >

< bmst >

References

Table 1. Description of different apple slice treatments

Condition #	Treatment	
	Pre-treatment	Drying Conditions
1	–	50°C
2	–	70°C
3	50°C HWB	50°C
4	70°C HWB	50°C
5	50°C HWB	70°C
6	70°C HWB	70°C
7	ASC + 70°C HWB	70°C
8	CIT + 70°C HWB	70°C
9	ASC + CIT + 50°C HWB	70°C
10	ASC + CIT + 70°C HWB	70°C

Table 2. Performance of moisture content PLSR models

Condition	Full Spectrum				Reduced (3-wavelength set)			
	Calibration		Test		Calibration		Test	
	r^2	RMSE (g/g) *[M.C. %]*	r^2	RMSE (g/g) *[M.C. %]*	r^2	RMSE (g/g) *[M.C. %]*	r^2	RMSE (g/g) *[M.C. %]*
1	1.00	0.01 *[0.12]*	1.00	0.11 *[1.32]*	0.99	0.18 *[2.16]*	1.00	0.09 *[1.08]*
2	1.00	0.03 *[0.36]*	1.00	0.07 *[0.84]*	1.00	0.18 *[2.16]*	0.98	0.05 *[0.60]*
3	1.00	0.04 *[0.48]*	0.92	0.68 *[8.16]*	0.99	0.22 *[2.64]*	0.98	0.15 *[1.80]*
4	1.00	0.05 *[0.60]*	1.00	0.17 *[2.04]*	0.99	0.27 *[3.24]*	1.00	0.05 *[0.60]*
5	1.00	0.03 *[0.36]*	0.95	0.43 *[5.16]*	0.99	0.22 *[2.64]*	0.97	0.28 *[3.36]*
6	1.00	0.05 *[0.60]*	0.99	0.19 *[2.28]*	0.99	0.25 *[3.00]*	0.99	0.16 *[1.92]*
7	1.00	0.02 *[0.24]*	0.95	0.70 *[8.40]*	0.99	0.20 *[2.40]*	0.98	0.29 *[3.48]*
8	1.00	0.04 *[0.48]*	0.99	0.20 *[2.40]*	0.99	0.24 *[2.88]*	0.99	0.08 *[0.96]*

9	1.00	0.06 *[0.72]*	0.99	0.18 *[2.16]*	0.99	0.27 *[3.24]*	0.99	0.08 *[0.96]*
10	1.00	0.08 *[0.96]*	1.00	0.11 *[1.32]*	0.99	0.27 *[3.24]*	0.99	0.09 *[1.08]*
Average	1.00	0.04 *[0.48]*	0.98	0.28 *[3.36]*	0.99	0.23 *[2.76]*	0.99	0.13 *[1.56]*

Table 3. Performance of CIELAB a* PLSR models

Condition	Full Spectrum				Reduced (2-component)			
	Calibration		Test		Calibration		Test	
	r^2	RMSE	r^2	RMSE	r^2	RMSE	r^2	RMSE
1	1.00	0.10	0.99	0.25	0.97	0.44	0.98	0.24
2	1.00	0.100	0.99	0.29	0.96	0.41	0.98	0.34
3	1.00	0.08	0.96	0.46	0.97	0.40	0.97	0.40
4	1.00	0.12	0.98	0.35	0.96	0.44	0.98	0.20
5	1.00	0.06	0.95	0.48	0.97	0.38	0.96	0.42
6	1.00	0.13	0.97	0.52	0.96	0.42	0.98	0.31
7	1.00	0.12	0.84	0.80	0.97	0.38	0.94	0.40
8	1.00	0.10	0.65	0.85	0.98	0.36	0.86	0.35
9	1.00	0.11	0.99	0.25	0.97	0.39	0.96	0.41
10	1.00	0.11	0.98	0.32	0.97	0.42	0.97	0.25
Average	1.00	0.10	0.93	0.46	0.97	0.40	0.96	0.33

Table 4. Performance of CIELAB b* PLSR models

Condition	Full Spectrum				Reduced (5-component)			
	Calibration		Test		Calibration		Test	
	r^2	RMSE	r^2	RMSE	r^2	RMSE	r^2	RMSE
1	0.98	0.52	0.93	0.48	0.94	0.81	0.72	0.00
2	0.97	0.46	0.96	0.67	0.93	0.74	0.86	0.00
3	0.97	0.57	0.89	0.56	0.91	1.01	0.81	0.18
4	0.98	0.43	0.95	0.79	0.92	0.93	0.86	0.09
5	0.99	0.40	0.89	0.99	0.95	0.74	0.73	0.74
6	0.98	0.43	0.94	0.75	0.95	0.80	0.79	0.63
7	0.99	0.42	0.90	0.89	0.95	0.79	0.76	0.15
8	0.98	0.51	0.97	0.53	0.92	0.95	0.85	0.16
9	0.99	0.39	0.92	0.94	0.97	0.57	0.77	1.06
10	0.98	0.47	0.90	0.97	0.93	0.94	0.85	0.13
Average	0.98	0.46	0.93	0.76	0.94	0.83	0.80	0.31

Table 5. Apple slice moisture content (gW/gDM)

Condition #	Treatment	Drying Conditions	Moisture content (g Water/g D.M) ± STDEV at different drying time (minutes)								
	Pre-treatment		0	30	60	90	120	150	180	240	300
1	–	50°C	7.56 ± 0.12	5.38 ± 0.19	3.88 ± 0.22	2.66 ± 0.23	1.55 ± 0.22	0.76 ± 0.19	0.36 ± 0.10	0.19 ± 0.02	
2	–	70°C	6.65 ± 0.11	4.87 ± 0.43	3.2 ± 0.51	1.83 ± 0.53	0.81 ± 0.39	0.27 ± 0.11	0.16 ± 0.03	0.12 ± 0.01	
3	50°C HWB	50°C	6.54 ± 0.11	5.09 ± 0.14	3.23 ± 0.14	2.01 ± 0.1	1.06 ± 0.07	0.44 ± 0.03	0.24 ± 0.01	0.17 ± 0.01	0.16 ± 0.01
4	70°C HWB	50°C	8.03 ± 0.14	5.81 ± 0.14	4.34 ± 0.09	2.94 ± 0.09	1.83 ± 0.13	0.96 ± 0.14	0.46 ± 0.08	0.21 ± 0.02	0.18 ± 0.02

5	50°C HWB	70°C	7.61 ± 0.11	4.22 ± 0.1	1.79 ± 0.09	0.42 ± 0.04	0.17 ± 0.01	0.14 ± 0.01	0.12 ± 0.01	0.11 ± 0.01	0.11 ± 0.01
6	70°C HWB	70°C	8.69 ± 0.32	4.87 ± 0.2	2.56 ± 0.15	0.74 ± 0.1	0.18 ± 0.02	0.14 ± 0.01	0.13 ± 0.01	0.12 ± 0.01	0.11 ± 0.01
7	ASC + 70°C HWB	70°C	8.03 ± 0.14	4.25 ± 0.27	1.64 ± 0.26	0.34 ± 0.1	0.16 ± 0.02	0.14 ± 0.02	0.13 ± 0.01	0.12 ± 0.01	0.11 ± 0.01
8	CIT + 70°C HWB	70°C	8.01 ± 0.28	4.78 ± 0.08	2.64 ± 0.13	1.03 ± 0.15	0.25 ± 0.05	0.15 ± 0.02	0.14 ± 0.01	0.12 ± 0.01	0.11 ± 0.01
9	ASC + CIT + 50°C HWB	70°C	7.74 ± 0.08	3.87 ± 0.2	1.61 ± 0.16	0.41 ± 0.07	0.16 ± 0.02	0.14 ± 0.01	0.12 ± 0.01	0.11 ± 0.01	0.11 ± 0.01
10	ASC + CIT +	70°C	7.22 ±	4.47 ±	2.67 ±	1.19 ±	0.37 ±	0.18 ±	0.15 ±	0.13 ±	0.12 ±

	70°C HWB		0.81	0.57	0.36	0.18	0.12	0.02	0.01	0.01	0.01

Figure 1. Emission spectra of the halogen light source. (Note that the fluctuations in spectrum are typical of halogen bulb spectra.)

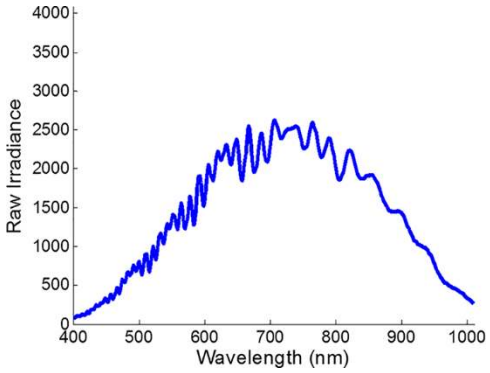

Figure 2. Basic imaging layout. The translation stage moves horizontally in the direction shown, allowing single scan lines to be acquired sequentially by the camera from the apple slice. a) Hyperspectral camera; b) halogen light source; c) direction of movement (30 cm scan length); d) white reference; e) apple slice.

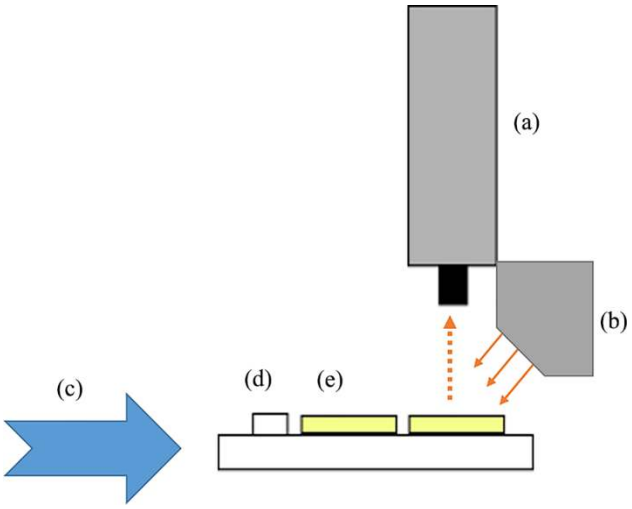

Figure 3. Segmentation of complete raw image. a) Original RGB image; b) the NIR thresholded image; and c) the blob-detected image for the automatic detection and numbering of imaged samples.

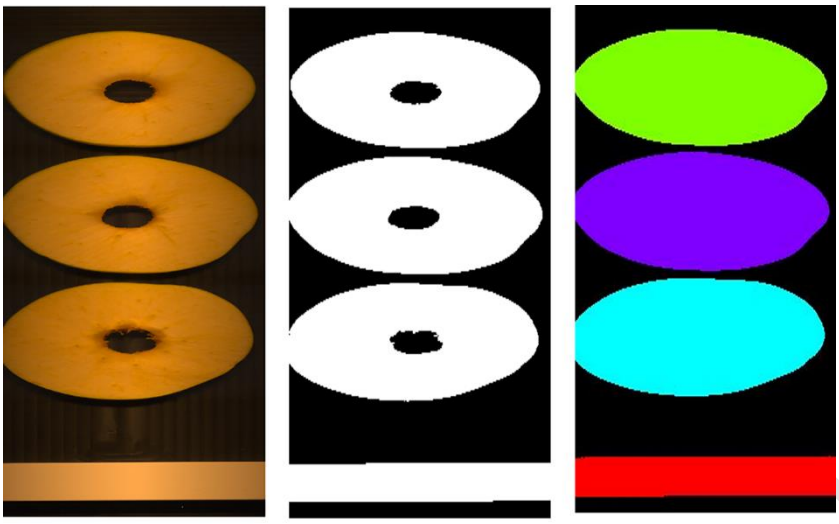

(a) (b) (c)

Figure 4. Average reflectance spectra of the apple slices for different treatment conditions and at different time points during the drying process: a) 0 minutes; and b) 180 minutes. Different coloured lines correspond to different treatments, labelled as in the legend, and itemised in Table 1.

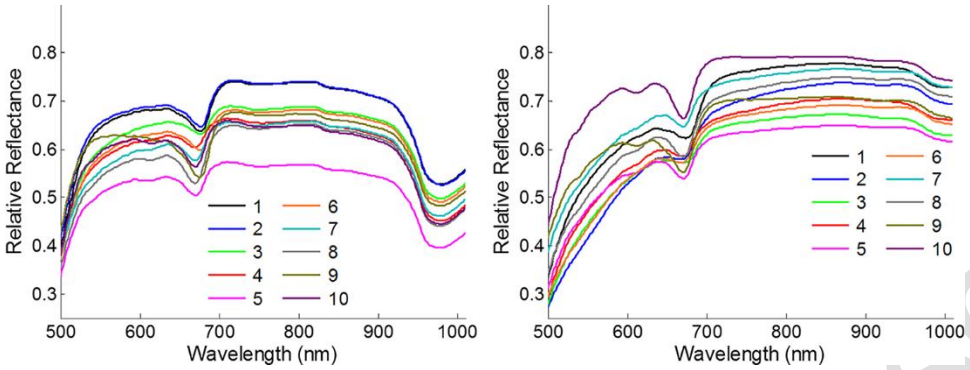

Figure 5. Illustration of a) changes in spectral reflectance for apples dried at 50°C (treatment condition 1) across different time points, corresponding to different coloured lines as in the legend, and b) the loading function for the moisture content prediction PLSR model with 4 components for each of the 10 apple treatment conditions.

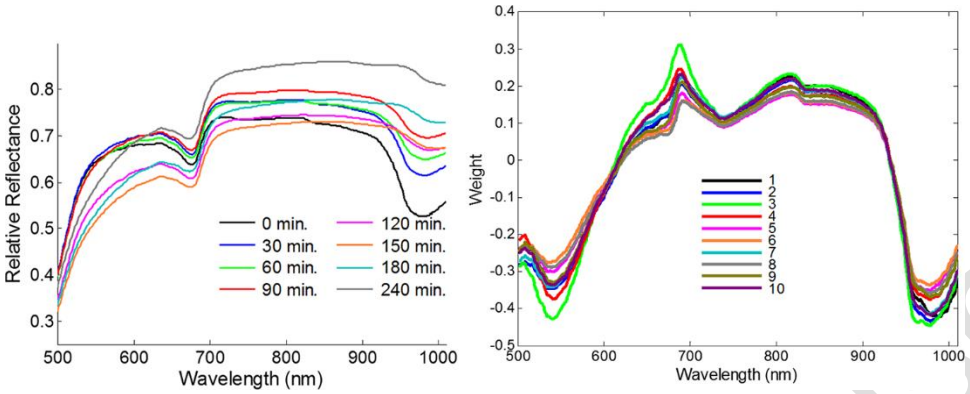

Figure 6. The a) drying curve for apple treatment Condition 7; Ascorbic acid and HWB at 70°C and b) comparison of the actual and predicted moisture content.

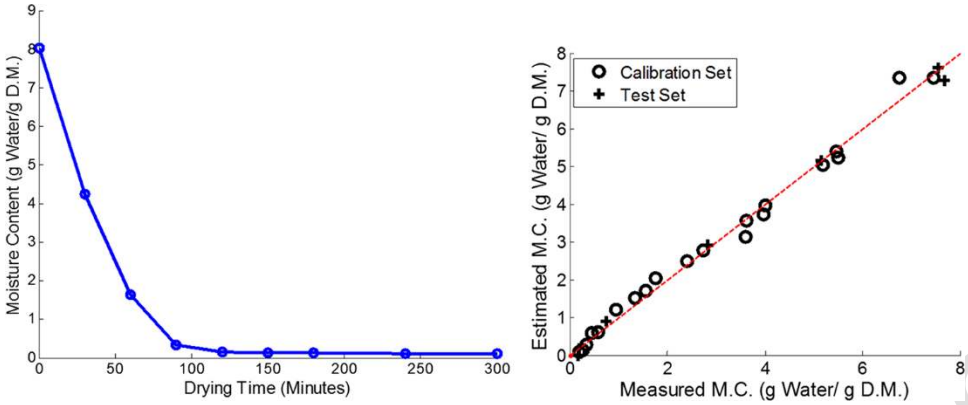

Figure 7. Images of a single apple slice at two different drying times. At 0 minutes (prior to drying): a) the sRGB image generated from the original hyperspectral image and pseudo colour images for b) moisture content [where 0 = 0 g_W/g_{DM}, 1 = 11.2 g_W/g_{DM} (extreme predicted value of < 10 pixels)], c) CIELAB a*, and d) CIELAB b*. After 60 minutes of drying at 50 oC: e) – h), with image types in the same order as the left-hand column.